On the interaction between two oppositely signed, shielded, monopolar vortices

On the interaction between two oppositely signed, shielded, monopolar vortices

M. R. Schmidt
Risø National Laboratory, Department of Optics and Fluid Dynamics, P.O. Box 49, DK-4000 Roskilde, Denmark

M. Beckers
Fluid Dynamics Laboratory, Department of Physics, Eindhoven University of Technology, P.O. Box 513, 5600 MB Eindhoven, The Netherlands

A. H. Nielsen and J. Juul Rasmussen
Risø National Laboratory, Department of Optics and Fluid Dynamics, P.O. Box 49, DK-4000 Roskilde, Denmark

G. J. F. van Heijst
Fluid Dynamics Laboratory, Department of Physics, Eindhoven University of Technology, P.O. Box 513, 5600 MB Eindhoven, The Netherlands

(Received 4 November 1997; accepted 31 August 1998)

The formation two-dimensional dipolar vortices by the interaction between two shielded monopolar vortices with opposite vorticity, as shown in a numerical study by Couder and Basdevant,[1] is investigated in detail, both experimentally, in a nonrotating stratified fluid and numerically by direct solutions of the two-dimensional Navier–Stokes equations. A comparative study between the laboratory experiments and numerical simulations is performed. The vorticity distribution measured in the early stage of the evolution in the laboratory is used as initial data for the simulations, and an additional damping term in the Navier–Stokes equations, that accounts for the vertical diffusion in the laboratory experiments, is used. The results show that, depending on the initial separation between the vortices, the shields of the monopoles are peeled off and indeed a compact dipole with a linear (ω,ψ)-relationship is formed, or when the monopoles are further apart the shields of the monopoles are perturbed and two tripoles are formed. The characteristics of the emerged dipole are analyzed and a dye visualization of the dipole formation is performed. A second, more general numerical study yields a relationship between the formation time of the dipole and the initial separation distance between the monopoles and it shows that the deshielding process can be explained by the domination of strain over vorticity. © *1998 American Institute of Physics.* [S1070-6631(98)02212-0]

I. INTRODUCTION

Vortical structures are known to be characteristic features of quasi two-dimensional flow systems.[2,3] Geophysical flows can be described by such a two-dimensional flow and both in the oceans of the Earth and in the atmospheres of the planets there are numerous observations of these vortical structures. The simplest and most commonly observed structure is the *monopolar vortex*, with a circular or elliptic shape and swirling motion of one orientation, examples of which are the high- or low-pressure cells in the atmosphere or the oceanic eddies.[4] The next is the *dipolar vortex*[5] which consists of two closely packed regions of opposite vorticity (i.e., two monopolar vortices). Also a *tripolar vortex*[6] is found to exist. It consists of an elliptically shaped core vortex with two satellites of opposite vorticity. The tripole and the monopole have angular momentum and rotate steadily around their core. The dipole has a net linear momentum, which makes it propagate. The translation is caused by the mutual propelling effects of the poles. When the dipole is symmetric, the two poles are equal, with opposite vorticity distribution, and the structure propagates along a straight line. Asymmetric dipoles, with different vorticity distribution, can also be observed; these vortex structures propagate along a curved path.

This contribution is devoted to a detailed investigation of the formation of dipolar structures from interacting monopoles. Propagating dipolar vortices are easily excited in two-dimensional (2D) flows and they appear to be the universal outcome of any external forcing possessing a nonzero linear momentum. The formation and dynamics of dipolar vortex structures have been thoroughly investigated in rotating[7] as well as in stratified flows,[8–11] where the dominant dynamics are well approximated by a two-dimensional flow.[12] In these studies the dipoles were generated by horizontal injection of a jet of fluid. In rotating flows the cloud of the injected fluid self-organized into a pair of columnar oppositely signed vortices aligned parallel to the rotation axis, while in a stratified fluid a flat pancake-like dipolar vortex structure is formed after the cloud of injected fluid collapses as a result of the buoyancy force.

In a numerical study it was observed by Couder and

Basdevant[1] (in this paper referred to as C&B) that two shielded, oppositely rotating monopolar vortices can also develop into compact dipoles, whereas the interaction between two nonshielded vortices only results in a weakly connected dipole. The shielding was found to provide an effective mechanism in bringing the vortex cores closer together. In laboratory experiments it was found that monopolar vortices in a nonrotating stratified fluid are always characterized by a shielded vorticity structure.[12–14] Therefore, the interaction between two oppositely signed monopolar vortices in a stratified fluid provides a way to study the formation process of a compact dipole as described by C&B in detail. Furthermore, the interaction of vortices in a stratified fluid can, as described in the present work, be compared with results from purely 2D numerical simulations.

Previous studies, numerical as well as experimental,[13,15–17] have shown that shielded monopolar (i.e., axisymmetric) vortices can be unstable, both in purely two-dimensional flows and in laboratory experiments with rotating homogeneous fluids and nonrotating stratified fluids. In this paper we not only investigate in detail the interaction of two oppositely signed shielded monopolar vortices and their re-organization into two dipoles, but we also show that the presence of the other vortex can perturb a shielded monopolar vortex, resulting in the formation of a tripole.

We first present a comparative study between experiments performed in a tank with a nonrotating stratified fluid, and purely two-dimensional numerical simulations. The purpose is to investigate how well the two-dimensional model reveals the dynamics observed in the laboratory experiment, and besides, to describe the dipole formation process in more detail. In the experiments the shielded monopoles are generated by a horizontal injection of an amount of fluid along the inner walls of two separate horizontal metal rings at the interface between salt and fresh water in a two-layer stratified fluid. At this interface, where the vortex motion takes place, vertical motion is inhibited. The two monopoles are formed and allowed to interact, after the removal of the confining rings. The flow evolution was visualized both by dye and by tracer particles floating at the fluid interface, making qualitative as well as quantitative analysis possible.

A close comparison between the laboratory experiments and numerical simulations was possible by using the experimentally measured spatial distribution of the vertical vorticity at the interface as initial condition for a program that integrates the two-dimensional, incompressible Navier–Stokes equations. An additional linear Rayleigh damping term was used to model the diffusion of vorticity in the direction perpendicular to the vortex motion, as the numerical code only solves the two-dimensional Navier–Stokes equations. Comparing the development of the isocontours of the vorticity we observe excellent agreement of the large scale dynamics, between the experiments and the simulations, despite the idealized model.

In addition, we briefly discuss results from a more general numerical study of the re-organization of interacting oppositely rotating monopoles in two-dimensional flows. In this part of the paper the linear damping term is, therefore, neglected in the model. These results are used for the analysis of the ''de-shielding'' process of the two shielded monopolar structures. The relation between the separation distance of two shielded Gaussian monopoles, and the formation time of a dipolar structure is investigated. It is found that two different exponential regimes exist, depending on the details of the de-shielding process: either the shielding is shed off in a continuous process, or two tripolar structures emerge as a transient state before the final formation of the dipole.

The paper is organized as follows: In Sec. II we describe the experimental setup and the results from three laboratory experiments. In Sec. III we describe the numerical model and the results from the simulations corresponding directly to the laboratory experiments. In Sec. IV we discuss the re-organization process in two-dimensional flows by using results from a more general numerical study. Finally, Sec. V contains the conclusions.

II. EXPERIMENTAL RESULTS

In this section we present the results of three different laboratory experiments performed in a tank with dimensions $l\times w\times h=89\times 39\times 40$ cm^3 filled with a two-layer (fresh and salt water) stratified fluid. The purpose of the experiments is to investigate the interaction behavior of two flat pancake-like shielded monopolar vortices of opposite vorticity. The monopolar vortices described in this paper are generated by the so-called tangential injection method,[13] in which an amount of fluid of matching density is injected horizontally along the inner wall of a small cylinder at the height of the density interface. After the injection of the fluid is stopped, the flow inside the cylinder is allowed to adjust to a purely circular motion (during a time τ), after which the cylinder is carefully lifted and removed from the tank.

A. Experimental arrangement

Trieling and van Heijst[14] have studied the decay of monopolar vortices, created by using the above described method, in a stratified fluid. They found that the vortices were in good agreement with the shielded Gaussian vortex model, i.e., the stream function (ψ) has a radially Gaussian distribution. The vertical vorticity (ω_z) distribution is characterized by a circular core region surrounded by a ring of opposite vorticity. The reason for the presence of this ring of opposite vorticity is twofold. The no-slip condition for the flow along the inner wall of the cylinder causes the generation of oppositely signed vorticity. Furthermore Beckers *et al.*[12] have shown that the ring of oppositely signed vorticity results from the fact that vortex lines of pancake-like vortices form closed loops. This implies that for monopoles there is always a ring of oppositely signed vertical vorticity present. It was shown by Flór and van Heijst[13] that this ring may be subject to instabilities, resulting in the formation of a tripolar vortex or even higher-order modes like a triangularly shaped core surrounded by three satellite vortices. In the experiments described here two shielded monopolar vortices, but with opposite sense of rotation, are generated simultaneously, closely together.

Figure 1 gives a sketch of the experimental set-up.

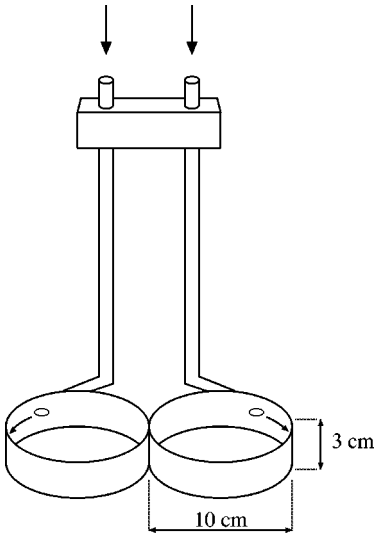

FIG. 1. Sketch of the experimental setup. Fluid is injected from above through the tubes at a rate Q and flows tangentially into the cylinders, along the inner walls, in opposite directions.

Through the tubes fluid of intermediate density is injected at the interface of the two-layer fluid. The injection is controlled by a stepmotor-driven mechanism that pushes a number of syringes at an adjustable speed. In this way the total volume (ΔV) and the injection rate (Q) can be varied. A third parameter that can be changed is the relative separation distance (d/R), with $R=5$ cm the radius of one cylinder, between the centers of the vortices. Typically twenty seconds after the injection is stopped the cylinders are lifted together by hand. During this elevation care is taken that the cylinders are lifted vertically in order to prevent the vortices from being vertically sheared by motion induced at higher levels. The lifting should also be very slowly, in order to prevent the generation of internal waves that may influence the motion at the interface of the step-wise stratification. In order to avoid these disturbing effects, the elevation speed should be no larger than ~ 1 cm s^{-1}, therefore, the removal of the cylinders from the tank takes typically 40 s.

To obtain quantitative information of the velocity field of the vortex structures, small, neutrally buoyant, polystyrene particles (of about 1 mm in diameter) are added to the fluid and float at the interface between the layers of fresh and salt water. These particles are illuminated by a light sheet, produced by slide projectors. Above the tank a video camera is mounted, to record the particle motions on video tape. After the experiments the tape can be processed using the *DigImage*-system[18] to determine the horizontal velocity field of the fluid at the interface as indicated by the passive tracer motion. When this velocity field is interpolated on a rectangular grid by a spline interpolation method,[19] the vertical vorticity ω_z and stream function ψ can be calculated at each grid point. The velocity field, therefore, needs to be averaged over a time interval of typically five to ten seconds, depending on the velocity magnitude of the flow.

We will describe three different laboratory experiments. In two experiments passive tracer particles are used to study the evolution of the vorticity during the interactions. In a third experiment dyed fluid is injected inside the cylinders, to visualize the advection of a passive tracer. We will refer to the particle experiments by the letters *A* and *B*. The experimental conditions of the dye-visualization experiment are equal to those in the particle-experiment *A*. In these experiments two vortices are generated at the closest possible distance: The cylinders are put against each other, viz. $d/R=2.0$. In experiment *B* the distance between the vortices was $d/R=2.9$. In all three experiments time is initialised at the start of the fluid injection. After the cylinders are lifted out of the fluid, Particle Tracking (i.e., velocity data acquisition by tracking the neutrally buoyant particles) is started. Table I enumerates all the experimental parameters.

TABLE I. Experimental parameters: Experiment name, relative separation distance (d/R), injected volume per vortex (ΔV), injection rate (Q), injection duration (Δt), adjustment time (τ), start of particle tracking (after the start of the injection) (t^*).

Exp.	d/R	ΔV (ml)	Q (ml s^{-1})	Δt (s)	τ (s)	t^* (s)
A	2.0	60	3.67	16.2	20	75
dye	2.0	60	3.67	16.2	20	···
B	2.9	60	3.00	20.0	20	80

B. Experiment *A*: Dipole formation

In Fig. 2 horizontal cross sections of the vertical vorticity at the interface are shown for experiment *A* at six different times. For clearness only the vorticity contours for $|\omega| \leqslant 0.082$ s^{-1} are shown, with a vorticity interval $\Delta\omega = 0.018$ s^{-1}. The positive vorticity values are represented by full contours, the negative values by the dashed contours. The shields at the outer boundary of the vortex system are

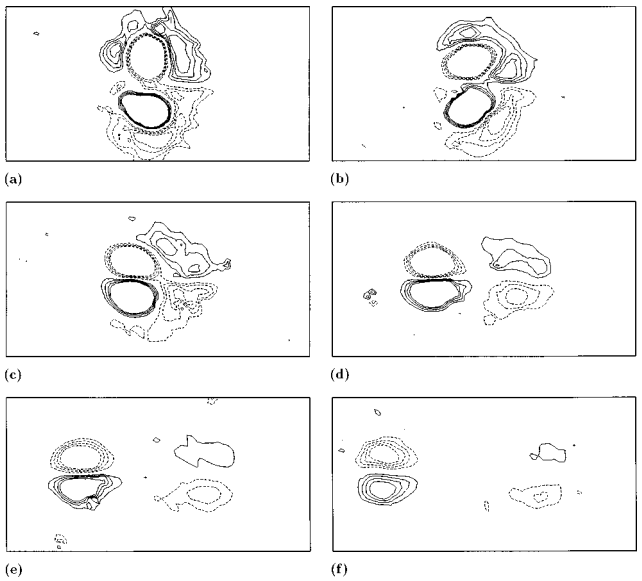

FIG. 2. Vorticity contours of experiment *A*. The domain sizes are 31 and 67 cm in the y and x directions, respectively. The injection rate was $Q=3.67$ ml s^{-1} and the injection volume per vortex $\Delta V=60.0$ ml. The data are plotted for (a) $t=85$ s, (b) $t=105$ s, (c) $t=135$ s, (d) $t=175$ s, (e) $t=225$ s, (f) $t=285$ s. The contours levels are $\Delta\omega=0.018$ s^{-1} for $|\omega| \leqslant 0.082$ s^{-1}. Continuous contours indicate positive vorticity, dashed contours negative vorticity.

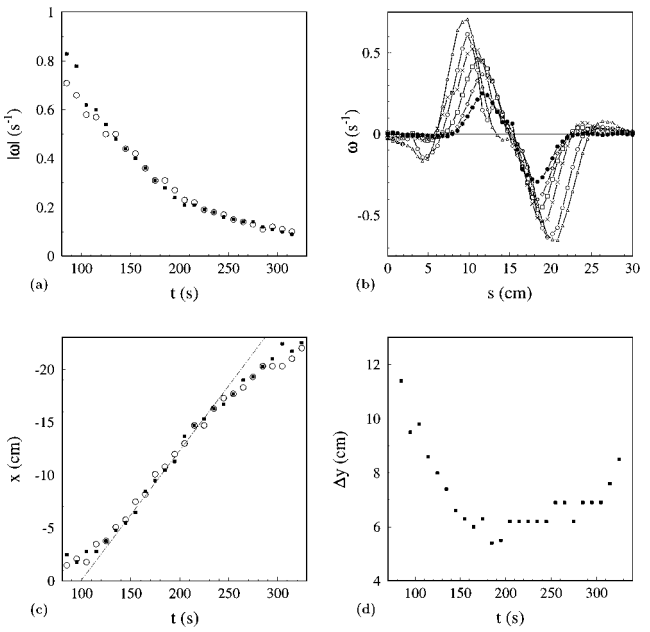

FIG. 3. Experiment *A*: (a) Maximum vorticity plotted against time for both vortex cores. Squares indicate the positive vorticity, circles the negative vorticity. (b) Cross sections (comoving with the dipole) of the vorticity along a line through the vorticity extrema for different times: △ $t=85$ s, ○ $t=95$ s, × $t=115$ s, □ $t=135$ s, ◇ $t=155$ s, ● $t=185$ s. (c) Horizontal position (x) of the vorticity extrema of the dipole plotted against time (t). Squares indicate the positive vorticity, circles the negative vorticity. (d) Distance between the vorticity extrema (Δy) for the dipole plotted against time.

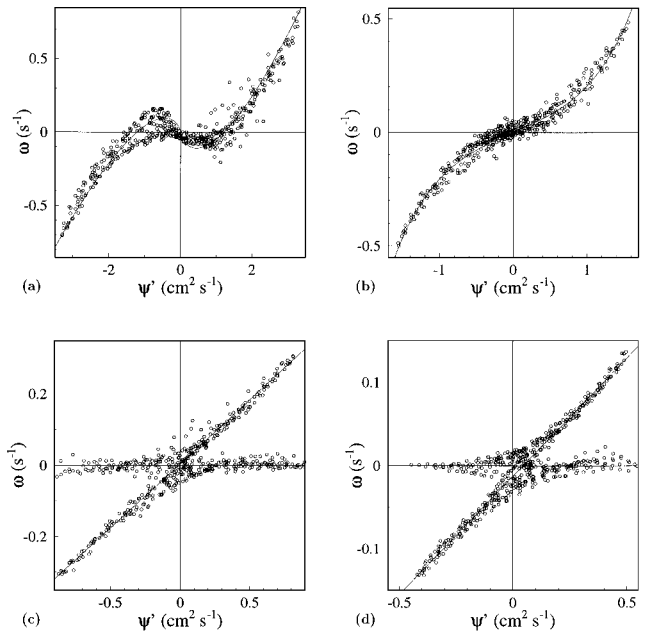

FIG. 4. Experiment *A*: (ω,ψ')-scatter plots for different times: (a) $t=85$ s, (b) $t=135$ s, (c) $t=175$ s, (d) $t=275$ s. The stream function ψ' has been corrected for the translation of the primary dipole. The velocities used here are (a) $U=0$, (b) $U=-0.09$ cm s^{-1}, (c) $U=-0.15$ cm s^{-1}, (d) $U=-0.09$ cm s^{-1}.

observed to be deformed by the vortex cores, and are advected to one side of the vortex system. Similarly to what was found in the numerical simulation by C&B the vortex cores undergo a change in shape, while being pressed together: Each core changes from rather circular [in Fig. 2(a)] to almost semicircular [in Fig. 2(d)]. In this latter stage they have formed together a vortex dipole, that starts to translate by its self-propelling mechanism, leaving behind the vorticity patches from the shielding. Shortly after its formation this vortex dipole has a tail structure, most likely caused by the straining effect of the remaining vorticity patches originating from the shielding. This effect has been described in a numerical study by Kida *et al.*[20] and in laboratory experiments by Trieling *et al.*[21] Not only the vortex cores form a dipole structure, but also the vorticity patches originating from the shielding start to move together as a dipole structure in the opposite direction, but at a much slower speed than the main dipole, because the vorticity values in the shielding are much smaller and the vorticity patches are more separated.

Figure 3(a) shows the decay of the maximum vorticity values of both vortex cores. The experimental error in these measurements is of the order of a few percent and is mainly caused by the averaging of vorticity values over grid elements of finite size. The decay of the vortices is caused by diffusion of momentum in the direction perpendicular to the flow field.[12–14] It can be seen that the positive vortex (represented by the squares) is only initially slightly stronger than the negative vortex (circles), and therefore the dipole moves in a straight path after it has been formed (i.e., after $t \approx 150$ s). To obtain more detailed information on the dipole, we focus on a smaller region of the domain moving with the dipole. Figure 3(b) shows the cross sections of the vorticity (moving with the vorticity extrema) through the dipole centres. Besides the decrease of the absolute vorticity we find that both vorticity extrema shift closer together. After $t \approx 115$ s the vorticity cross sections of the dipole show a continuous vorticity distribution between the cores. The observation that from $t=155$ s the distance between the vorticity extrema remains approximately unchanged also indicates that the formation of the dipole is completed at $t \approx 150$ s. The positions and separation distance of the vorticity extrema in Figs. 3(c) and 3(d), respectively, both reveal three stages in the life of the dipole. From $t=85$ s until $t=150$ s the translation speed U increases and the core separation Δy decreases; this is the formation stage of the dipole. Then in the second stage, approximately from $t=150$ s to $t=250$ s, the separation distance reaches a minimum and the translation velocity a maximum. In the third stage entrainment of ambient irrotational fluid into the dipole structure and the decrease of the dipole's strength, due to vertical diffusion, lead to a further decrease in the translation velocity and an increase again in the core separation distance.

The translation velocity U of the main dipole is estimated to calculate the stream function $\psi'=\psi-Uy$, in a frame comoving with the dipole. This is achieved by minimizing the scatter on the (ω,ψ')-relationship, while changing the velocity U as a free parameter. The corrected stream function is plotted against vorticity in Fig. 4 for four different times in the dipole formation process. The vorticity and stream function data have been calculated on a domain moving with the dipole. At $t=85$ s [Fig. 4(a)] no correction for

translation was made, as the vortices did not yet move at that stage. Clearly two separate branches, each characteristic for a shielded monopole, are visible in this stage. Each branch is compared separately to the shielded Gaussian vortex model for a monopolar vortex given by

$$\omega = 2\psi(1+\ln(2\psi)). \tag{1}$$

Besides the scatter for the part representing the shielding, a reasonable agreement can be observed between the data and the Gaussian models. In Fig. 4(b), the (ω,ψ')-scatter plot at $t=135$ s is plotted, with $U=-0.09$ cm s^{-1}. The line shown here is a sinh-function fitted to the data. This function appears to be a good representation of the shape of the scatter plot at this moment of the dipole formation. In their numerical simulations C&B have shown that dipoles which have a weak linkage between the two vortex patches possess such a nonlinear (ω,ψ)-relationship, like the dipole structure that results from the interaction between two nonshielded monopoles. Flór and van Heijst[9] found that dipoles that result from the turbulent injection of an amount of fluid in a stratified fluid also possess such a nonlinear (ω,ψ')-relationship. These dipoles also showed a slight shift between the two vortex halves. Apparently, the present dipole structure at $t=135$ s, which has not yet formed a compact dipole can be characterized by the same (ω,ψ')-relationship very well. C&B also showed in their simulations that such a nonlinear dipole can transform into a linear one [i.e., with a linear (ω,ψ')-relationship], when the two vortex halves are compressed. They indicated that such a compression can be obtained by the presence of an oppositely signed shielding around the nonlinear dipole, as created in the present experiment, or by an oblique collision between two of such ''nonlinear dipoles.''

Indeed the vortex dipole in the present experiment gradually transforms into a linear one visible from approximately $t=175$ s. This linear (ω,ψ')-relationship remains unchanged, only the vorticity and stream function values decrease in time. At $t=175$ s [Fig. 4(c)] and $t=275$ s [Fig. 4(d)] the dipole structure is compared to the Lamb dipole model, characterized by a linear relationship between the vorticity and the stream function in a frame comoving with the dipole and valid within a circle of radius a

$$\omega = k^2\psi'. \tag{2}$$

The value for k^2 has been determined from the least-squares fits in Figs. 4(c) and 4(d), giving $k^2=0.36$ cm^{-2} and $k^2=0.29$ cm^{-2} at $t=175$ s and $t=275$ s, respectively. The vorticity distribution of the dipole model, which can be found by solving the Poisson equation $\omega=-\nabla^2\psi$, is given by (see, e.g., Batchelor[22])

$$\omega = \frac{2kU}{J_0(ka)}J_1(kr)\sin\theta \quad \text{for} \quad r\leqslant a, \tag{3}$$

whereas $\omega=0$ outside the dipole. U is the translation velocity of the dipole, θ the azimuthal coordinate measured from the dipole's axis and J_1 the first Bessel function of the first kind. Continuity at $r=a$ requires that $ka=3.83$ and outside the circle $r=a$ the Bessel function is truncated, so that the external flow is irrotational. The value for k can be determined by the slope of the (ω,ψ')-scatter plot. The decrease in the value of k can be interpreted as due to an increase of the radial size a of the dipole, as the product ka indicates the position of the first zero of J_1. Although the Lamb model is not a realistic model (due to the Bessel function truncation at its first zero), a main characteristic of the Lamb dipole can clearly be observed in the experimental data, namely the linear relationship between the vorticity and the stream function. In addition, the decrease of the slope of this relationship in time is associated with a radial growth of the dipole, in correspondence with the model's dispersion relation.

C. Dye visualization

Figure 5 presents six photographs of the dye visualization experiment of two interacting shielded monopoles, performed under the same experimental conditions as in experiment *A*. The fluids injected in the cylinders were dyed with different colours. The times at which the photographs in Figs. 5(a)–5(e) were taken, correspond with those of the vorticity plots of experiment *A* in Figs. 2(a)–2(e). The presence of oppositely signed vorticity along the edge of both vortex cores is obvious by the rolling up of fluid originally located at the front of the vortex system [as can be seen in Figs. 5(b) and 5(c)]. Also the vortex cores transform from a circular shape [Fig. 5(a)] towards semicircles [Fig. 5(d)]. From $t\approx 220$ s an opening is formed at the rear of the dipole, indicating that undyed fluid is entrained into the dipole. When comparing the dye visualization and experiment *A* (which is believed to be allowed because the experimental conditions are approximately the same), it is seen in Fig. 3(d) (by the increase of the separation distance) that the entrainment starts around $t\approx 250$ s, which corresponds with the observation in the dye visualization shown in Fig. 5. Furthermore, in Fig. 3(c) one can see that the velocity starts to decrease around $t\approx 230$ s, indicating the entrainment of irrotational fluid into the dipole at approximately the same time. Unfortunately, in this experiment the resulting primary dipole is slightly asymmetric in strength, as can be inferred from its slightly curved path.

D. Experiment *B*: No dipole formation

In experiment *B* the cylinders were placed at an initial separation $d/R=2.9$. Figure 6 shows the contour plots of the vertical vorticity of experiment *B* at six different times. Already in the first vorticity plot at $t=90$ s it can be seen that both vortex cores tend to become elliptical, while the rings of opposite vorticity of each vortex split up into two separate satellite vortices. The separation between the vortex cores enables two of the satellites to ''slip through'' them [see Fig. 6(c)]. An equivalent formation of tripoles in the interaction of like-signed shielded monopoles has been found in numerical simulations of shielded vortex merger by Carton[23] and Carton and Bertrand.[24] It is unclear whether the instability of both experimental vortices is caused by the mutual influence of the vortices, because it was shown by Flór and van Heijst[13] that also a single monopole, generated by the tangential injection method, could become unstable and form a

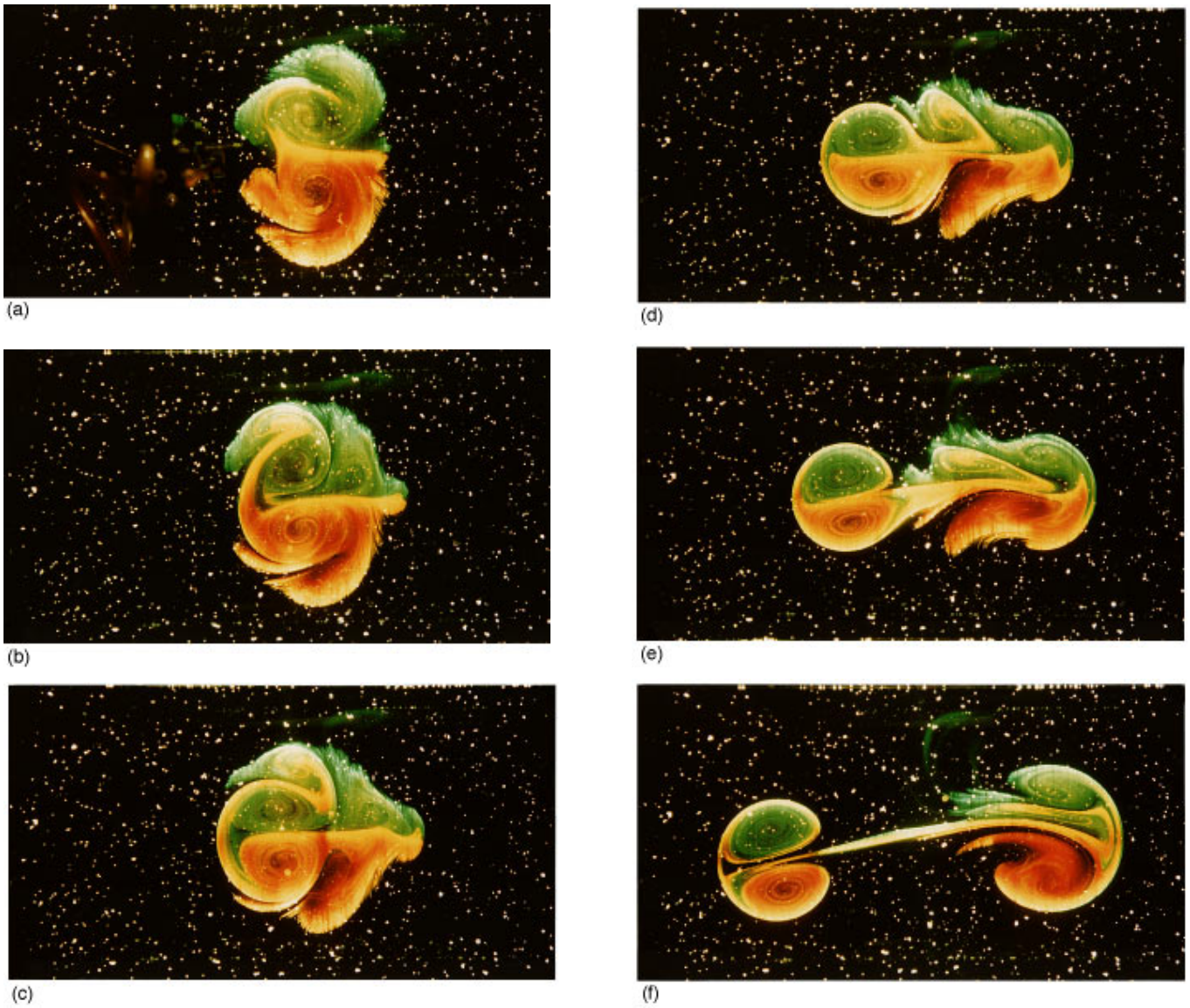

FIG. 5. Photographs of a visualization experiment using the injection of dyed fluid. Red dye for the anti-clockwise rotating vortex, green dye for the clockwise rotating vortex. The pictures are taken at (a) $t=90$ s, (b) $t=105$ s, (c) $t=134$ s, (d) $t=173$ s, (e) $t=221$ s, (f) $t=387$ s after the injection of fluid started. The injection rate was $Q=3.67$ ml s^{-1} and the injection volume per vortex $\Delta V=60.0$ ml. Times and experimental parameters are comparable to experiment *A*.

tripole. It is, however, reasonable to assume that each monopole perturbs the other, thereby perhaps triggering the instability.

For this experiment a similar decay (due to vertical diffusion) has been observed as for experiment *A* shown in Fig. 3(a). The negative vortex was found to be slightly weaker than the positive one during the whole experiment. This probably resulted in the slower rotation of the satellites around the negative core compared to the positive core as can be seen in Figs. 6(c)–6(e). In contrast to experiment *A* no translation of the vortex system is observed in a direction perpendicular to the axis connecting both vortex cores. In other words, no compact dipole is formed. The (ω,ψ)-relationship maintains the same characteristic shape for two separate independent shielded structures, as the one shown in Fig. 4(a), during the complete flow evolution.

III. NUMERICAL RESULTS

A. Model and numerical setup

To describe the vortex dynamics in the experiments discussed in the previous section we employ a simplified model based on the two-dimensional incompressible Navier–Stokes equations. The equations include an additional friction term, which is introduced to account for the ''dissipation'' due to the vertical diffusion. In the experiments vorticity diffuses vertically, effectively damping the fluid motion at the interface in a much stronger way than would be the case in a purely two-dimensional flow. To fully describe this mechanism one has to incorporate the effect of vertical diffusion, which results, in a three-dimensional model.[12–14] In the simplified two-dimensional model employed here a linear Rayleigh friction accounts for the viscous damping in a direc-

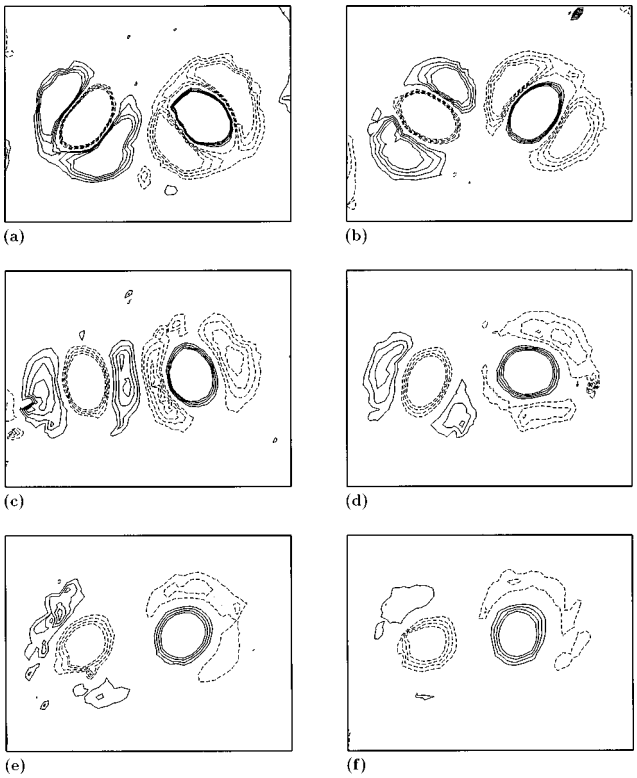

FIG. 6. Vorticity contours of experiment *B*. The domain sizes are 29 and 38 cm in the y and x directions, respectively. The injection rate was $Q=3.00\ \mathrm{ml\ s^{-1}}$ and the injection volume per vortex $\Delta V=60.0$ ml. The data are plotted for (a) $t=90$ s, (b) $t=130$ s, (c) $t=170$ s, (d) $t=210$ s, (e) $t=250$ s, (f) $t=290$ s. The contours levels are $\Delta\omega=0.018\ \mathrm{s^{-1}}$ for $|\omega|\leqslant 0.082\ \mathrm{s^{-1}}$. Continuous contours indicate positive vorticity, dashed contours negative vorticity.

tion perpendicular to the fluid interface. In the vorticity—stream function formulation the equations read:

$$\frac{\partial\omega}{\partial t}+J\{\omega,\psi\}=\nu\nabla^2\omega-\lambda\omega, \tag{4}$$

$$\nabla^2\psi=-\omega, \tag{5}$$

where ω is the vertical component of vorticity, ψ is the stream function, ν is the kinematic viscosity, and the term λ is the Rayleigh friction coefficient. J designates the Jacobian, defined by $J\{\omega,\psi\}=(\partial\omega/\partial x)(\partial\psi/\partial y)-(\partial\omega/\partial y)(\partial\psi/\partial x)$. The velocity field is related to the stream function as

$$u=\frac{\partial\psi}{\partial y},\quad v=-\frac{\partial\psi}{\partial x}. \tag{6}$$

We have solved Eqs. (4) and (5) numerically in a double periodic domain, with size $L_x\times L_y$, using a standard, fully de-aliased spectral scheme, with a resolution of $M\times N$ $(M/L_x=N/L_y)$. The dynamics is only insignificantly influenced by the periodicity, when the field is vanishing near the borders of the computational domain, i.e., the typical scale size of the structures is much smaller than size of the domain. Time integration was performed by a third order Adams–Bashforth explicit scheme for the Jacobian, and a backward Euler scheme for the damping terms.

In the first series of simulations, where the results from the experiments (*A* and *B*) are used as initial conditions, we have used the parameters: $\nu=0.01\ \mathrm{cm^2\ s^{-1}}$ (approximately the viscosity of water at 20 °C) and $\lambda=5\cdot 10^{-3}\ \mathrm{s^{-1}}$, resulting in a time scale of vorticity decay as observed in the experiments [see Fig. 3(a)]. The experimentally obtained vorticity distribution can be interpolated to a regular grid by digital image analysis [see Sec. II A]; furthermore this grid can be interpolated to finer grids and larger domains, e.g., by employing Fourier analysis. We call a regular, interpolated grid an ''experimental array.'' The computational grid is taken larger than the experimental array, in order to avoid the influence from the periodic boundaries. The values at the grid points outside the experimental array are set to zero. Thus, along the border between the experimentally obtained array and the remaining grid, the field is discontinuous, which will introduce some numerical noise due to the Gibbs phenomenon. However, the level of this noise is at least one order of magnitude smaller than the experimental noise, and the sharp gradients at the borders are rapidly smoothened out by the viscosity. Thus, differences between the experiments and the simulations should only be due to mechanisms which are not modelled by Eqs. (4) and (5). The domain is quadratic in both simulations, with size $L_x=L_y=42.66$ cm and a resolution in each direction of $M=N=256$ grid points.

In a second series of simulations, we have investigated the formation of dipoles from more generalized monopolar structures—both shielded and unshielded. As initial data for the shielded structures we have chosen two equal monopoles of opposite sign with Gaussian-shaped stream functions. Thus, the initial stream function of the total system is given by

$$\psi(x,y)=A\ \exp\left(-\frac{(x+x_0)^2+y^2}{2r_0^2}\right)-A\times\exp\left(-\frac{(x-x_0)^2+y^2}{2r_0^2}\right), \tag{7}$$

which yields the vorticity field

$$\omega(x,y)=A\left\{\frac{(x-x_0)^2+y^2}{r_0^4}-\frac{2}{r_0^2}\right\}\exp\left(-\frac{(x-x_0)^2+y^2}{2r_0^2}\right)-A\left\{\frac{(x+x_0)^2+y^2}{r_0^4}-\frac{2}{r_0^2}\right\}\times\exp\left(-\frac{(x+x_0)^2+y^2}{2r_0^2}\right), \tag{8}$$

with r_0 the radius of the Gaussian and x_0 half the separation distance between the cores. (Note that r_0 is in general smaller than the radius of the cylinder R: it was found experimentally that $d/r_0\approx 2.3d/R$.) The initial data for an unshielded structure is a Gaussian-shaped distribution of the vorticity, i.e., the total system has a vorticity field with the form similar to that in Eq. (7).

Furthermore, we have employed vortex models for isolated monopolar vortex structures as proposed by Carton

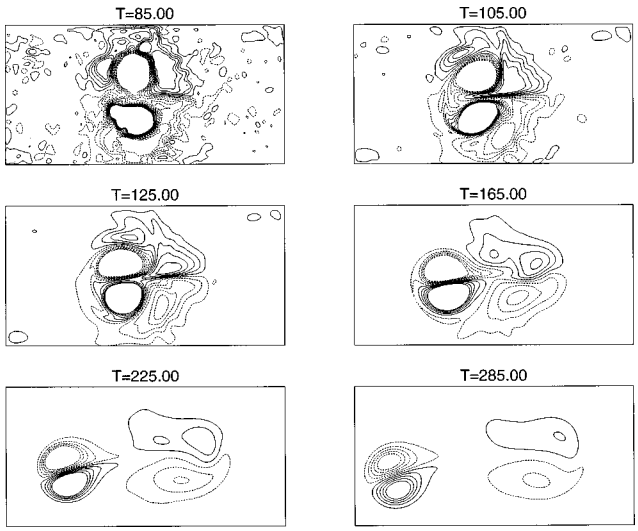

FIG. 7. Simulation *A*: Vorticity contour plots. Dashed contours correspond to negative values and continuous contours correspond to positive values. The lowest and highest contours correspond to $\omega=-0.082\ \mathrm{s}^{-1}$ and $\omega=0.082\ \mathrm{s}^{-1}$ respectively. The contour interval is $0.018\ \mathrm{s}^{-1}$.

et al.[16] These models are characterized by a velocity and vorticity profile for each of the axisymmetric monopoles of the form of a stretched Gaussian

$$v_\theta(r,\theta;\alpha)=\tfrac{1}{2}r\ \exp(-r^\alpha),$$
$$\omega(r,\theta;\alpha)=[1-\tfrac{1}{2}\alpha r^\alpha]\exp(-r^\alpha), \tag{9}$$

where v_θ is the azimuthal velocity and r a dimensionless radial coordinate. The variable α is a tuning parameter that controls the steepness of the profiles. For vortices in laboratory experiments, using generation techniques discussed in Sec. II, values of α have been measured[9,13] in the range between 1 and 2. The monopolar vortices described by this model have a zero total circulation, for every value of α.

B. Simulation *A*: Dipole formation

Here we present a simulation corresponding to experiment *A*. The experimental array is 192 by 96 grid points. The initial data are obtained from the vorticity field in the experiment at $t=85$ s, and the evolution of the vorticity corresponding to Fig. 2 is shown in Fig. 7 using the same contour levels of the vorticity. Only the experimental array is shown, as the field is nearly zero in the remaining part of the computational domain. Initially, a range of small scale structures is present, but they are rapidly damped. Already at the start of the simulation, the shielding is partly removed. Thus, a dipole is rapidly formed from the two cores of the initially shielded monopoles. The de-shielding is asymmetric, leading to an oblique trajectory of the emerging structure. However, this structure is quite well shaped at the end of the simulation. The faster decay of the strong (positive) core, visible in Fig. 8(a), indicates that the formed dipole becomes more symmetric, so that the dipole trajectory tends to become rectilinear after $t\approx 200$ s. The simulated evolution is in quite close agreement with the experimental observations. In Fig. 8(b) the vorticity profiles, taken along a cross section through the centers of the dipole halves, are shown and it is observed that the emerging dipole is symmetric and compact as it has a continuous vorticity distribution between the two dipole halves.

Also the vorticity patches originating from the shielding tend to form a large dipole, see Fig. 7, moving in the direction opposite to the primary dipole, in agreement with the

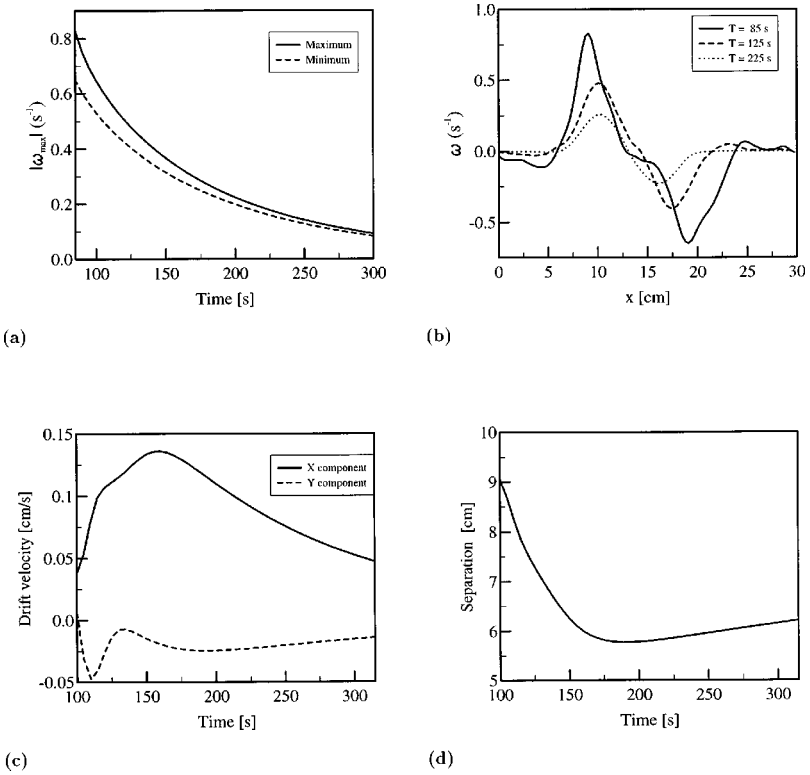

FIG. 8. Simulation *A*: (a) The absolute value of maximum and minimum vorticity (the peak values of the cores) plotted as a function of time. (b) Cross sections of vorticity along a line through the two extrema points. (c) The *x* and *y* components of the drift velocity for the center point of the system, as a function of time. The center point is defined as the center point of the maximum and minimum vorticity. (d) The separation distance as a function of time. The separation distance is defined by the distance between the peak values of the two cores (maximum and minimum vorticity).

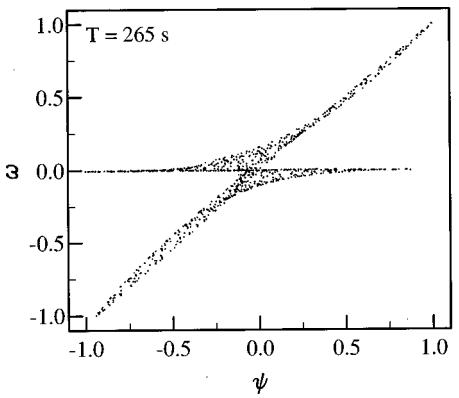

FIG. 9. Simulation *A*: (ω,ψ')-scatter plot of the dipole structure. Both quantities have been scaled by their extrema values. The stream function has been corrected for the translation of the dipolar structure (drift speed of the center point), see Fig. 8(c).

observations in Fig. 2. However, this structure is damped before obtaining a significant drift velocity. Figures 8(c) and 8(d) show the drift velocity and the separation distance of the emerging dipole. Both quantities are calculated using the peak positions. These quantities allow us to estimate the formation time of the emerging dipole, either defined as the time for the maximum drift velocity, or as the time for the minimum separation distance. Using the first criterion, we observe that the formation is completed around $t=160$ s, from Fig. 8(c). Using the second criterion, the formation is completed around $t=185$ s, see Fig. 8(d).

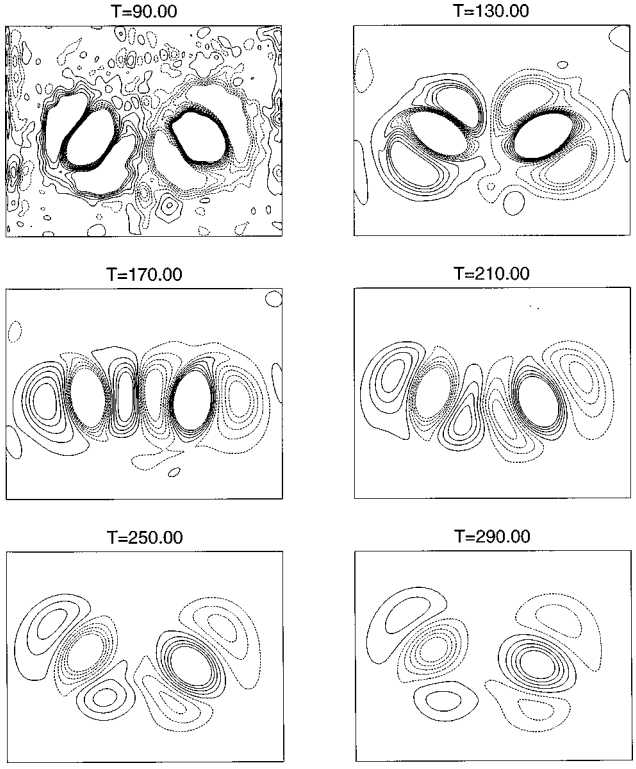

FIG. 10. Simulation *B*: Vorticity contour plots. Dashed contours correspond to negative values and continuous contours correspond to positive values. The lowest and highest contours correspond to $\omega=-0.082\ \mathrm{s}^{-1}$ and $\omega=0.082\ \mathrm{s}^{-1}$, respectively. The contour interval is $0.018\ \mathrm{s}^{-1}$.

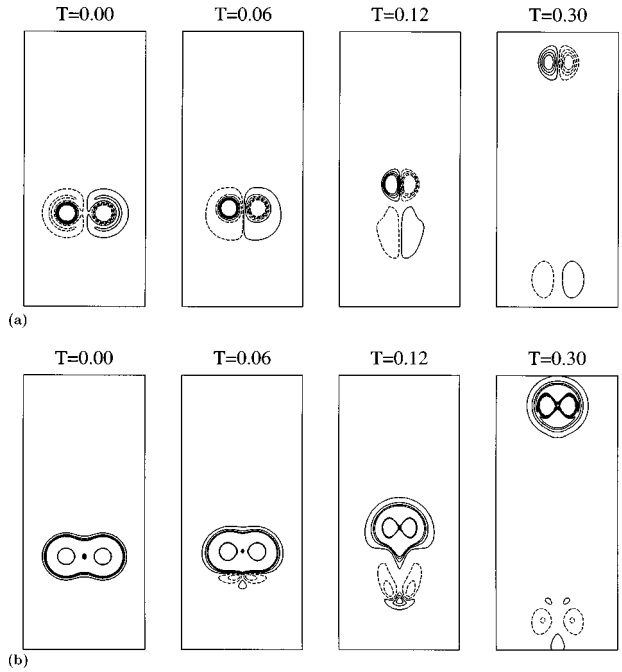

FIG. 11. Results of simulations in which initially two shielded Gaussian monopoles of opposite vorticity are superimposed. Dashed contours correspond to negative vorticity values and continuous contours correspond to positive values. (a) Vorticity contour plots. The lowest and highest contours correspond to $\omega=-310$ and $\omega=310$, respectively. The contour interval is 69. (b) Weiss field contour plots. The lowest and highest contours correspond to $Q=-3000$ and $Q=3000$, respectively. The contour interval is 666. Both quantities as well as the time are in dimensionless units. The parameters are $A=1$, $x_0=0.11$, $r_0=0.05$ corresponding to $T_R=0.0078$, and $\nu=2\cdot10^{-3}$. The computational domain is $L_x=1$, $L_y=4$, ($M=256$, $N=1024$), but only part of it is shown in the figure.

Figure 9 shows the (ω,ψ')-scatter plot at $t=265$ s inside a circle following the center point of the dipole. At this time a nearly linear relationship between the vorticity and the stream function is observed, in agreement with Fig. 4(d), characterizing a Lamb type dipole.[22]

C. Simulation *B*: No dipole formation

Here we present a simulation corresponding to experiment *B*. The initial data for the numerical solution are obtained from the experimentally determined vorticity field at $t=90$ s. The experimental array consists of 228 by 174 grid points. In Fig. 10 we show the evolution of the vorticity distribution of simulation *B* for the same times as shown in Fig. 6 and again using the same contour levels of the vorticity. Like in the previous simulation the small scale structures that are initially present are quickly damped and the two large-scale structures, the tripoles, become more smooth throughout the simulation. However, they continuously perturb each other, and the small difference in the initial strength leads to different rotation rates of the satellites around the two vortex cores. As in the experiment, the accumulated effect seems to be a loss of symmetry in the system.

Finally, we monitored the (ω,ψ)-relationship in the simulation at various times and compared it with the experiment. Qualitatively, the scatter plots from the simulation are found to be similar to the experimentally observed ones and are not

shown here. In both simulations (*A* and *B*) it is found that the linear damping term describes the decay of the vortices due to vertical diffusion to a large extent and the large-scale dynamics in the experiment and the simulation show a good agreement.

IV. ANALYSIS OF THE DESHIELDING PROCESS

To understand the general formation of dipoles from two nearby monopolar vortices, we performed simulations employing various initial conditions ranging from shielded vortices described by a Gaussian stream function, Eq. (7), over ''stretched Gaussians,'' defined by Eq. (9), to unshielded vortices given by Gaussian vorticity profiles. For these calculations we omitted the Rayleigh damping term, and retained only the kinematic viscosity term in Eq. (4). For the shielded case (Gaussian stream function) we observed the ultimate formation of a compact dipole of Lamb type with a linear relationship between ω and ψ, whenever the mutual distance of the two initial vortices was below a critical distance. A typical example is shown in Fig. 11(a) for a case with moderate viscosity, expressed in terms of the Reynolds number of the emerging dipole, $Re=(dU)/\nu\approx 240$, where U is the translation speed and d is the distance between the extrema of the two poles just after the formation of the dipole. All quantities are measured in dimensionless units; characteristic parameters are given in the figure caption. We have chosen an elongated computational domain: $L_x=1$, $L_y=4$, and $\nu=2\cdot 10^{-3}$. The remaining parameters are $A=1$, $x_0=0.11$, and $r_0=0.05$. After a time corresponding to ~ 10 internal turnover times, where the internal turnover time is defined from the maximum vorticity $T_R=2\pi/\omega_{\max}$, the cores of the two initial monopoles start to escape their shielding and move away forming a compact dipolar structure. The distance d between the centers of the poles is significantly smaller than the initial distance $2x_0$. Shortly after the escape the cores form a compact, strongly interacting dipolar structure, which is steadily propagating. The dipole has a nearly perfect circular outer boundary outside which the vorticity is zero, except for a small tail emerging at the rear of the dipole. The corresponding scatter plot shows a perfect linear relationship between the stream function and the vorticity. The evolution observed in Fig. 11(a) is similar to the evolution shown in Figs. 2 and 7. The shield is smeared off and a compact dipole with a Lamb-dipole-like structure emerges. The dipole then propagates while slowly being dissipated as described for a Lamb dipole.[25–27]

The de-shielding process may be understood by following the evolution of the so-called Weiss field, see Weiss.[28] This field represents the spatial distribution of the quantity Q, that is defined by

$$Q=\tfrac{1}{4}(s^2-\omega^2), \tag{10}$$

where s is the strain rate $s=[(u_x-v_y)^2+(u_y+v_x)^2]^{1/2}$ and ω is the vorticity. The quantity Q can thus be used to separate the flow into strain dominated regions, where $Q>0$, and vorticity dominated regions where $Q<0$. From the evolution of Q in Fig. 11(b) we observe that in the region around the two monopolar vortices, i.e., in the region of the shielding, the flow is strongly strain dominated, which results in a rapid deformation in this region. Thus, the vorticity shielding is strongly elongated and this results ultimately in the removal of the shield and in the compression effect on the two monopoles bringing them together to form a compact dipole. The straining field between the two vortices tends to draw out smaller ''necks'' of the vorticity dominated region [second frame in Fig. 11(b)] which indicate an attraction. The vorticity originating from the shielding forms a weak noncompact dipole moving in the opposite direction. Note also the characteristic form of the Weiss field for the mature dipole, which shows strong straining around the stagnation points at each end of the dipole. The Weiss field inside the dipole is strongly negative, and can therefore not be seen with the present choice of contours.

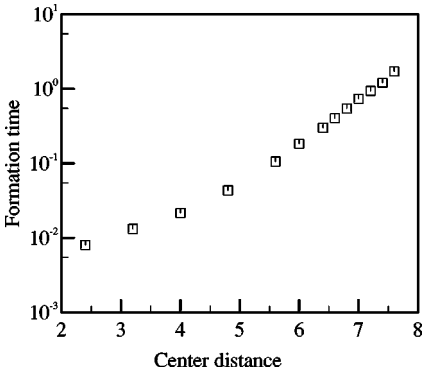

FIG. 12. The formation time of a dipolar structure from two equal, shielded monopoles with opposite vorticity as a function of their initial separation distance normalized with their initial radia $2x_0/r_0$. The parameters are $A=0.8$, $r_0=0.025$ corresponding to $T_R=0.0025$, and $\nu=2\cdot 10^{-5}$.

In Fig. 12 we have summarized the investigations of the dipole formation from two shielded monopoles (for purely two-dimensional cases without vertical diffusion). That is, for a specific vorticity distribution we have plotted the formation time versus the initial distance between the vortex centers. The distance is normalized by the radius of the shielded Gaussian monopole, r_0. The formation time is defined as the time when the dipole reaches the maximum velocity, or equivalently when the distance between the poles becomes minimum. It is unimportant which criterion is used, as the viscous damping is low compared to the simulations *A* and *B*. For the results in Fig. 12 we used a viscosity $\nu=2\cdot 10^{-5}$ and the maximum value of the vorticity in each pole was 2560, corresponding to an internal turnover time $T_R=0.0025$. The first observation, in Fig. 12, is that for small separations the formation time is approximately an exponential function of the relative distance. The next observation is that the semilog plot in fact shows two different exponential regimes. They meet around the relative distance 4.8. The different regimes are related to the details of the reorganization process. Actually there is also a third regime for $2x_0/r_0\geqslant 8$, where no dipole was observed to form within attainable computation time.

For values of $2x_0/r_0<4.8$ the distance between the two vortex cores decreases very fast and they move through their common shielding. For larger distances ($2x_0/r_0>4.8$), *tri-*

polar structures similar to those observed in Figs. 6 and 10 are created temporarily. The shielding around each of the poles is rolled up into a weaker ring and two smaller satellites. The formation of these tripolar structures delays the de-shielding process. However, the two satellites are not equal as they are exposed to different straining, the satellite between the cores is strongly deformed, the other is advected along the outer boundary of the core structure. This deformation creates filaments, which are absorbed by the second satellite. Ultimately, the two satellites merge, and at the next encounter with the satellite around the other core, a secondary dipole is formed that escapes the two core vortices, which then form the compact dipole, moving in the opposite direction. When the relative distance between the cores is large, the deformation of the satellites is smaller, and they have time to re-organize while they are advected. Thus, the formation time increases with separation distance.

It should be noted in this respect that the final distance between the cores of the compact dipole only depends weakly on the initial separation of the two monopoles. Changing the viscosity only changes the formation time moderately. When the viscosity is increased, we observe a slight decrease in the formation time.

C&B investigated the formation of dipoles from the interaction between both shielded and unshielded monopoles. They emphasized that a shielding of the initial monopoles is necessary to form the compact dipolar structure. This shielding acts as compressing the two original poles to form a more compact structure, as we saw above. To investigate the influence of the shielding we also considered the interaction between unshielded monopoles and never obtained compact dipoles. Investigation of the Weiss field in these simulations only showed weak straining in front and behind the two vortices, in contrast to the shielded case [see Fig. 11(b)].

This difference between the interaction of shielded vortices and the interaction of nonshielded vortices may be understood by invoking the conservation of energy. Two unshielded monopolar vortices cannot move closer, because this would lead to an decrease in the energy, while they have no possibility to compensate for this energy decrease. For unshielded vortices only their shape may change, i.e., they become more elongated, but this does not affect the amount of energy much. For shielded vortices, on the other hand, the rearrangement of the shields can compensate the energy change when the cores move closer together.

We have only considered symmetric initial conditions, i.e., the two vortices have opposite signs but have equal strengths. In all cases we observed the evolution of a symmetric dipole and we did not see any trace of the instability that appears for a dipole consisting of vortex patches as observed by Dritschel.[29] Thus this instability does not seem to appear for vortices with distributed vorticity.

Finally, we have performed extensive studies of the generalized, shielded structures, Eq. (9), with $\alpha=1.2$ and $\alpha=1.75$, and different combinations of viscosity and initial distance. They all yield the same results, in the sense that the shielding is unstable and a dipole emerges as the final state. However, the dipoles in these cases are less compact. The formation time and the final velocity, for a given initial distance depends on the specific value of α, but not in a critical manner. The crossover between the two exponential regimes, shown in Fig. 12, increases slowly as α decreases. The flatter profile of the shielding makes the roll-up process weaker compared to the deformation by the core, thereby inhibiting the transient formation of tripolar structures.

V. CONCLUSIONS

We have considered the formation of dipolar vortex structures from two interacting monopolar vortices. Laboratory experiments were conducted in a nonrotating stratified fluid, in which two monopolar vortices have been created by the tangential injection of fluid inside two cylinders at the interface between salt and fresh water. These vortices are essentially isolated (shielded). After the removal of the cylinder the vortices interacted and formed a compact dipolar vortex, while their vorticity shieldings were removed. The measured (ω,ψ')-relationship evolved towards a linear one during the dipole formation. In a second laboratory experiment the monopolar vortices were generated at a larger mutual separation distance and did not form a dipole, but perturbed each other resulting in the formation of two tripoles. These laboratory experiments were compared with numerical simulations that solve the two-dimensional Navier–Stokes equations, including an additional Rayleigh damping term. Laboratory measurements of the vorticity distribution were used as initial conditions. The evolution of the vortex structures in these numerical simulations showed a very close agreement with the laboratory observations, which indicates that the purely two-dimensional description with a linear damping term provides a good approximation of the flow in the experiment. Further numerical simulations using various initial conditions revealed that compact Lamb-like dipoles always form from two shielded monopoles when their mutual separation distance is smaller than a critical value. For larger distances an intermediate state of two counter rotating tripoles was found, which eventually resulted in the formation of a tripole. The formation time measured in terms of the internal turnover time depends exponentially on the initial distance (with different *e*-folding times for the two regimes) and only weakly on the viscosity. The deshielding process has been analysed by Weiss' criterion and it was found that in the region of the shielding the flow was strongly strain dominated, resulting in a rapid deformation in this region. When the interactions between shielded and nonshielded monopoles are compared it is concluded that the vorticity shielding provides the possibility for the necessary energy redistribution. This allows the two vortex cores to move closer together.

ACKNOWLEDGMENTS

We thank H. J. H. Clercx for his comments on an earlier version of the manuscript. One of us (M.B.) gratefully acknowledges financial support from the Dutch Foundation of Fundamental Research on Matter (FOM). Part of this project was supported by the Danish Natural Science Research Council (SNF).

[1]Y. Couder and C. Basdevant, ''Experimental and numerical study of vortex couples in two-dimensional flows,'' J. Fluid Mech. **173**, 225 (1986).
[2]J. C. McWilliams, ''The emergence of isolated coherent vortices in turbulent flows,'' J. Fluid Mech. **146**, 21 (1984).
[3]B. Legras, P. Santangelo, and R. Benzi, ''High-resolution numerical experiments for forced two-dimensional turbulence,'' Europhys. Lett. **3**, 811 (1988).
[4]J. C. McWilliams, ''Submesoscale, coherent vortices in the ocean,'' Rev. Geophys. **23**, 165 (1985).
[5]K. N. Fedorov and A. I. Ginsburg, ''Mushroom-like currents (vortex-dipoles): One of the most widespread forms of non-stationary coherent motions in the ocean,'' *Mesoscale/synoptic Coherent Structures in Geophysical Turbulence*, edited by J. C. J. Nihoul and B. M. Jamart (Elsevier, Amsterdam, The Netherlands, 1989), pp. 1–14.
[6]R. D. Pingree and B. LeCann, ''Three anticyclonic slope water oceanic eddies (swoddies) in the southern Bay of Biscay in 1990,'' Deep-Sea Res. **39**, 1147 (1992).
[7]E. J. Hopfinger and G. J. F. van Heijst, ''Vortices in rotating fluids,'' Annu. Rev. Fluid Mech. **25**, 241 (1993).
[8]G. J. F. van Heijst and J.-B. Flór, ''Dipole formation and collisions in a stratified fluid,'' Nature (London) **340**, 212 (1989).
[9]J.-B. Flór and G. J. F. van Heijst, ''An experimental study of dipolar structures in a stratified fluid,'' J. Fluid Mech. **279**, 101 (1994); J.-B. Flór, ''Coherent vortex structures in a stratified fluid,'' Ph.D. thesis, Eindhoven University of Technology, The Netherlands, 1994.
[10]J.-B. Flór, G. J. F. van Heijst, and R. Delfos, ''Decay of dipolar structures in a stratified fluid,'' Phys. Fluids **7**, 374 (1995).
[11]S. I. Voropayev and Y. D. Afanasyev, *Vortex Structures in a Stratified Fluid* (Chapman and Hall, London, United Kingdom, 1994).
[12]M. Beckers, R. Verzicco, H. J. H. Clercx, and G. J. F. van Heijst, ''The vertical structure of pancake-like vortices in a stratified fluid: experiments, theory and numerical simulations,'' J. Fluid Mech. (submitted).
[13]J.-B. Flór and G. J. F. van Heijst, ''Stable and unstable monopolar vortices in a stratified fluid,'' J. Fluid Mech. **311**, 257 (1996).
[14]R. R. Trieling and G. J. F. van Heijst, ''Decay of monopolar vortices in a stratified fluid,'' Fluid Dyn. Res. **23**, 27 (1998).
[15]G. J. F. van Heijst and R. C. Kloosterziel, ''Tripolar vortices in a rotating fluid,'' Nature (London) **338**, 569 (1989).
[16]X. J. Carton, G. R. Flierl, and L. M. Polvani, ''The generation of tripoles from unstable axisymmetric isolated vortex structures,'' Europhys. Lett. **9**, 339 (1989).
[17]P. Orlandi and G. J. F. van Heijst, ''Numerical simulation of tripolar vortices in 2D flow,'' Fluid Dyn. Res. **9**, 179 (1992).
[18]S. Dalziel, ''DigImage. Image Processing for Fluid Dynamics,'' Cambridge Environmental Research Consultants Ltd., 1992.
[19]J.-M. Nguyen Duc and J. Sommeria, ''Experimental characterization of steady two-dimensional vortex couples,'' J. Fluid Mech. **192**, 175 (1988).
[20]S. Kida, M. Takaoka, and F. Hussain, ''Formation of head-tail structures in a two-dimensional uniform straining flow,'' Phys. Fluids A **3**, 2688 (1991).
[21]R. R. Trieling, J. M. A. van Wesenbeeck, and G. J. F. van Heijst, ''Dipolar vortices in a strain flow,'' Phys. Fluids **10**, 144 (1998).
[22]G. K. Batchelor, *An Introduction to Fluid Mechanics* (Cambridge University Press, Cambridge, 1967).
[23]X. J. Carton, ''On the merger of shielded vortices,'' Europhys. Lett. **9**, 697 (1992).
[24]X. J. Carton and C. Bertrand, ''The influence of environmental parameters on two-dimensional vortex merger,'' in *Modelling of Ocean Vortices*, edited by G. J. F. van Heijst (Royal Netherlands Academy of Arts and Sciences, Amsterdam, 1993), pp. 125–134.
[25]A. H. Nielsen and J. Juul Rasmussen, ''Formation and temporal evolution of the Lamb-dipole,'' Phys. Fluids **9**, 982 (1997).
[26]G. E. Swaters, ''Viscous modulation of the Lamb dipole vortex,'' Phys. Fluids **31**, 2745 (1988).
[27]G. E. Swaters, ''Dynamical characteristics of decaying Lamb couples,'' J. Appl. Math. and Phys. (ZAMP) **42**, 109 (1991).
[28]J. Weiss, ''The dynamics of enstrophy transfer in two-dimensional hydrodynamics,'' Physica D **48**, 273 (1991).
[29]D. G. Dritschel, ''A general theory for two-dimensional vortex interactions,'' J. Fluid Mech. **293**, 269 (1995).